Efficient Algorithm for Many-Electron Angular Momentum and Spin Diagonalization on Atomic Subshells

Christian B. Mendl*

Zentrum Mathematik, Technische Universität München, Boltzmannstraße 3, 85748 Garching bei München, Germany.

Abstract. We devise an efficient algorithm for the symbolic calculation of irreducible angular momentum and spin (LS) eigenspaces within the n-fold antisymmetrized tensor product $\wedge^n V_u$, where n is the number of electrons and $u = \text{s,p,d,}\cdots$ denotes the atomic subshell. This is an essential step for dimension reduction in configuration-interaction (CI) methods applied to atomic many-electron quantum systems. The algorithm relies on the observation that each L_z eigenstate with maximal eigenvalue is also an L^2 eigenstate (equivalently for S_z and S^2), as well as the traversal of LS eigenstates using the lowering operators L_- and S_-. Iterative application to the remaining states in $\wedge^n V_u$ leads to an *implicit* simultaneous diagonalization. A detailed complexity analysis for fixed n and increasing subshell number u yields run time $\mathcal{O}(u^{3n-2})$. A symbolic computer algebra implementation is available online.

1 Introduction

Since the inception of quantum mechanics, it is well-known that the (non-relativistic, Born-Oppenheimer) Hamiltonian governing many-electron atoms leaves the simultaneous eigenspaces of the angular momentum, spin and parity (LS) operators

$$L^2, L_z, S^2, S_z, \hat{R} \tag{1.1}$$

invariant. From a practical perspective, the restriction to symmetry subspaces can significantly reduce computational costs (see, e.g., Refs. [1–4]). In particular, such a restriction

---

*Corresponding author. *Email address:* `mendl@ma.tum.de` (C. B. Mendl)

is an essential ingredient for configuration interaction (CI) approximation methods in Refs. [5–7]. However, simultaneous diagonalization of the operators (1.1) on the full CI space is encumbered by the inherent "curse of dimensionality", which renders "naive" $\mathcal{O}(\dim^3)$ approaches infeasible. The present paper outlines an efficient algorithm for computing the symbolic eigenspaces by making use of representation theory and the algebraic properties of the LS operators.

In (1.1), the total angular momentum operator is defined as $L = \sum_{j=1}^{n} L(j)$ with n the number of electrons and

$$L(j) = \frac{1}{\mathrm{i}} x_j \times \nabla_j \tag{1.2}$$

the angular momentum operator acting on electron j. (We choose units such that $\hbar = 1$.) L_z is the third component of L. In spherical polar coordinates, $L_z(j) = \frac{1}{\mathrm{i}} \partial/\partial \varphi_j$. Analogously for spin, $S = \sum_{j=1}^{n} S(j)$ with $S_\alpha(j)$ for $\alpha = x,y,z$ the usual Pauli matrices

$$\sigma_x = \frac{1}{2}\begin{pmatrix} 0 & 1 \\ 1 & 0 \end{pmatrix}, \quad \sigma_y = \frac{1}{2}\begin{pmatrix} 0 & -\mathrm{i} \\ \mathrm{i} & 0 \end{pmatrix}, \quad \sigma_z = \frac{1}{2}\begin{pmatrix} 1 & 0 \\ 0 & -1 \end{pmatrix} \tag{1.3}$$

acting on electron j. The components of the angular and spin operators obey the well-known commutator relations $[L_\alpha, L_\beta] = \mathrm{i} L_\gamma$ and $[S_\alpha, S_\beta] = \mathrm{i} S_\gamma$ with α, β, γ cyclic permutations of x,y,z. The *ladder operators* are given by $L_\pm = L_x \pm \mathrm{i} L_y$ and $S_\pm = S_x \pm \mathrm{i} S_y$. They have the property that for any angular momentum eigenfunction ψ^{m_ℓ} with eigenvalue m_ℓ, $L_\pm \psi^{m_\ell}$ is zero or an eigenfunction with eigenvalue $m_\ell \pm 1$, and correspondingly for spin. The *parity operator* acts on wavefunctions as $\hat{R}\psi(x_1, s_1, \cdots, x_n, s_n) = \psi(-x_1, s_1, \cdots, -x_n, s_n)$, where $x_j \in \mathbb{R}^3$ and $s_j \in \{-\frac{1}{2}, \frac{1}{2}\}$ are the position and spin coordinate of electron j.

The simultaneous diagonalization of the LS operators is greatly simplified by representation theory using Clebsch-Gordan coefficients. Specifically, the required computational cost is reduced to the calculation of irreducible LS representation spaces (i.e., diagonalizing the operators (1.1)) on the n-fold antisymmetrized tensor product $\wedge^n V_u$ (compare with Ref. [7, proposition 2]). Here, V_u denotes an angular momentum subshell, $u = \mathrm{s}, \mathrm{p}, \mathrm{d}, \mathrm{f}, \cdots$ in chemist's notation. An explicit realization of V_u is

$$V_u = \mathrm{span}\{Y_{u,m}\uparrow, Y_{u,m}\downarrow\}_{m=u,u-1,\cdots,-u} \tag{1.4}$$

with the spherical harmonics $Y_{u,m}$:

$$Y_{\mathrm{s},0} = \frac{1}{\sqrt{4\pi}},$$

$$Y_{\mathrm{p},1} = -\frac{1}{2}\sqrt{\frac{3}{2\pi}}\sin(\theta)\mathrm{e}^{\mathrm{i}\varphi}, \quad Y_{\mathrm{p},0} = \frac{1}{2}\sqrt{\frac{3}{\pi}}\cos(\theta), \quad Y_{\mathrm{p},-1} = \frac{1}{2}\sqrt{\frac{3}{2\pi}}\sin(\theta)\mathrm{e}^{-\mathrm{i}\varphi}$$

$$\cdots$$

We identify the subshell label u with the corresponding quantum number, i.e., $\mathrm{s}, \mathrm{p}, \mathrm{d}, \mathrm{f}, \cdots \leftrightarrow 0,1,2,3,\cdots$. In particular, $\dim(V_u) = 2(2u+1)$. Note that $Y_{u,m}\uparrow, Y_{u,m}\downarrow$ are simultaneous single-particle L_z-S_z eigenstates. They serve as underlying ordered orbitals, which we

denote abstractly as

$$
\begin{array}{ll}
(\text{s},\overline{\text{s}}) & \text{for } V_\text{s}, \\
(\text{p}_1,\overline{\text{p}_1},\text{p}_0,\overline{\text{p}_0},\text{p}_{-1},\overline{\text{p}_{-1}}) & \text{for } V_\text{p}, \\
(\text{d}_2,\overline{\text{d}_2},\text{d}_1,\overline{\text{d}_1},\cdots,\text{d}_{-2},\overline{\text{d}_{-2}}) & \text{for } V_\text{d}, \\
(\text{f}_3,\overline{\text{f}_3},\text{f}_2,\overline{\text{f}_2},\cdots,\text{f}_{-3},\overline{\text{f}_{-3}}) & \text{for } V_\text{f}, \\
\cdots &
\end{array}
$$

The highest L_z quantum number appears first, and $\overline{}$ equals spin down $\downarrow$, following the convention in Ref. [5]. The elements of $\wedge^n V_u$ are then linear combinations of Slater determinants built from these orbitals, for example $\frac{1}{\sqrt{2}}|\text{d}_2\overline{\text{d}_1}\text{d}_{-1}\rangle - \frac{i}{\sqrt{2}}|\text{d}_1\text{d}_0\overline{\text{d}_0}\rangle \in \wedge^3 V_\text{d}$.

The simultaneous diagonalization may now be formalized as follows. For a given $n \in \{1,2,\cdots,\dim(V_u)\}$, we need to decompose the n-particle space $\wedge^n V_u$ into irreducible LS representation spaces $V_{u,n,i}$,

$$\wedge^n V_u = \bigoplus_i V_{u,n,i} \tag{1.5}$$

such that

$$
\begin{aligned}
\boldsymbol{L}^2 \varphi &= \ell_i(\ell_i+1)\varphi, & L_\pm \varphi &\in V_{u,n,i}, \\
\boldsymbol{S}^2 \varphi &= s_i(s_i+1)\varphi, & S_\pm \varphi &\in V_{u,n,i} \quad \text{for all } \varphi \in V_{u,n,i}, \\
\dim(V_{u,n,i}) &= (2\ell_i+1)(2s_i+1). &
\end{aligned}
\tag{1.6}
$$

The proposed algorithm (see Section 2) performs the LS diagonalization implicitly, relies on the sparse matrix structure of the lowering operators L_-, S_-, and makes use of the algebraic structure of $\wedge^n V_u$ as illustrated in Fig. 1. We present explicit tables containing decompositions of selected $\wedge^n V_u$ in Section 3. Given u, the number of electrons maximizing $\dim(\wedge^n V_u) = \binom{\dim(V_u)}{n}$ equals $n = 2u+1$ since $\dim(V_u) = 2(2u+1)$. Due to this exponential growth in u, solving Eq. (1.5) for all possible n restricts u to the s, p and d subshells at present, and $u = \text{f}$ for all $n = 1,\cdots,14$ might still be attainable. On the other hand, keeping n fixed means that $\dim(\wedge^n V_u) = \mathcal{O}(u^n)$ asymptotically in u. For a given n the algorithm has run time

$$R_n(u) = \mathcal{O}\left(u^{3n-2}\right), \tag{1.7}$$

as derived in Section 4.1. In particular, for $n = 2$, this equals $\mathcal{O}(\dim(\wedge^n V_u)^2)$ (instead of $\mathcal{O}(\dim(\wedge^n V_u)^3)$ for the usual diagonalization of a dense matrix).

As an alternative scenario, consider the case that we are only interested in representation spaces $V_{u,n,i}$ with ℓ_i and s_i equal (or close to) zero. As our analysis will show, this opens up the possibility of explicitly diagonalizing (1.1) restricted to the "central" simultaneous L_z-S_z eigenspace with eigenvalues $(0,0)$ for n even and $(0,\frac{1}{2})$ for n odd, respectively. Due to symmetry, this eigenspace also has the highest dimension (denoted
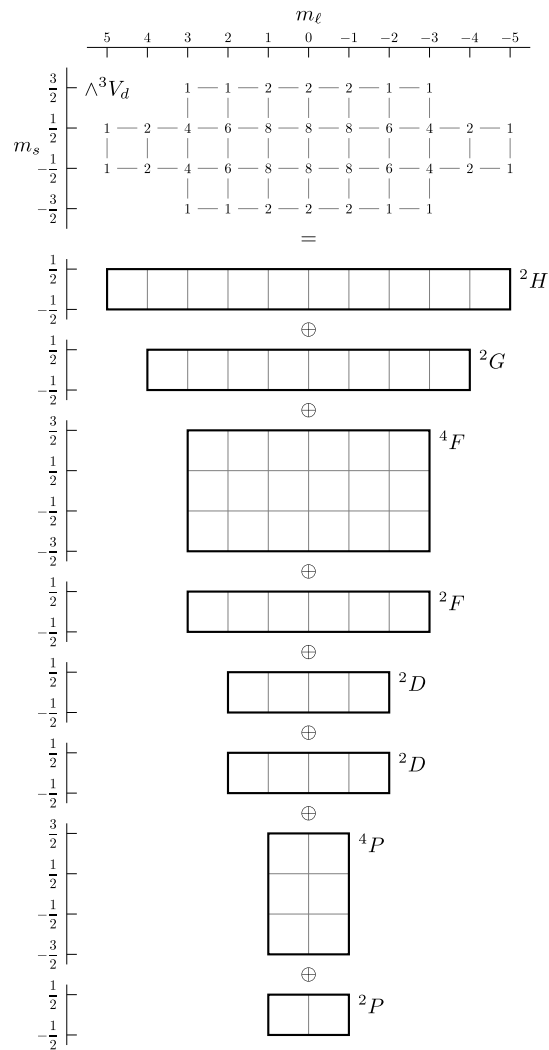
Figure 1: Algebraic decomposition of $\wedge^3 V_{\mathrm{d}}$ into irreducible LS representation spaces $V_{\mathrm{d},3,i}$ (see Eq. (1.5)). Each of these spaces corresponds to a rectangle, matching the m_ℓ and m_s quantum numbers running from $\ell_i, \cdots, -\ell_i$ and $s_i, \cdots, -s_i$, respectively. The (ℓ_i, s_i) quantum numbers are displayed in common chemist's notation as $^{2s+1}\ell$. Superimposing all rectangles yields the multiplicities of the L_z-S_z eigenvalues in the table at the top.

$d_{u,n}$) among all simultaneous L_z-S_z eigenspaces within $\wedge^n V_u$. In Section 4.2, we derive the asymptotic result

$$d_{u,n} \cong \sqrt{3}\, \frac{\dim(\wedge^n V_u)}{\pi n u} = \mathcal{O}(u^{n-1}) \quad \text{as } u \to \infty, \text{ for fixed } n. \tag{1.8}$$

Thus, diagonalization restricted to this central eigenspace still requires $\mathcal{O}(d_{u,n}^3) = \mathcal{O}(u^{3n-3})$ operations.

2 Algorithm

The reasoning and basic ingredients of our algorithm are as follows:

1. Observe that the canonical Slater determinant basis vectors of $\wedge^n V_u$ are precisely the eigenvectors of both L_z and S_z acting on $\wedge^n V_u$. For example, $L_z|d_2\overline{d_1}d_{-1}\rangle = (2+1-1)|d_2\overline{d_1}d_{-1}\rangle$ and $S_z|d_2\overline{d_1}d_{-1}\rangle = (\frac{1}{2}-\frac{1}{2}+\frac{1}{2})|d_2\overline{d_1}d_{-1}\rangle$. In particular, all simultaneous L_z-S_z eigen*values* can easily be enumerated, including multiplicities.

2. Let $\ell_{\max}$ be the largest L_z eigenvalue on $\wedge^n V_u$ and $W_{L_z,\max}$ the corresponding eigenspace, as well as $\psi \in W_{L_z,\max}\setminus\{0\}$. Then ψ must also be an $\boldsymbol{L}^2$ eigenvector with eigenvalue $\ell_{\max}(\ell_{\max}+1)$. This follows from the identity

$$\boldsymbol{L}^2 = L_z(L_z+\boldsymbol{1}) + L_-L_+ \tag{2.1}$$

    and the fact that L_+ is zero on $W_{L_z,\max}$ since $\ell_{\max}$ is – by definition – the largest L_z eigenvalue. The same reasoning applies to S_z and $\boldsymbol{S}^2$ restricted to $W_{L_z,\max}$. Thus we may assume that ψ is also a S_z-$\boldsymbol{S}^2$ eigenvector with eigenvalue s and $s(s+1)$, respectively.

3. Starting from ψ, we may span an irreducible LS representation space V_ψ by repeatedly applying the lowering operators L_- and S_-. That is, $V_\psi := \mathrm{span}\{\psi, L_-\psi, S_-\psi, L_-S_-\psi, \cdots\}$.

4. We obtain all remaining irreducible representation spaces by iteratively applying steps 2 and 3 to the orthogonal complement of V_ψ in $\wedge^n V_u$.

Algorithm 1 Quantum numbers of all irreducible subspaces in $\wedge^n V_u$

1: Enumerate the simultaneous eigenvalues of L_z and S_z acting on $\wedge^n V_u$, including multiplicities, and store them in a table denoted T_z. For example, figure 1 shows the multiplicity table for $\wedge^3 V_d$.

2: $i \leftarrow 1$

3: **while** T_z contains non-zero multiplicities **do**

4:      Let $\ell := \ell_{\max}$ be the greatest L_z eigenvalue in T_z with non-zero multiplicity, and let s be a corresponding S_z eigenvalue which is maximal among all tuples $(\ell_{\max}, s)$ in T_z.

5:      Calculate the m_ℓ and m_s quantum numbers corresponding to (ℓ, s), i.e., the tuples (m_ℓ, m_s) for all $m_\ell = \ell, \cdots, -\ell$ and $m_s = s, \cdots, -s$. Decrement the multiplicity of each (m_ℓ, m_s) in T_z by one.

6:      $(\ell_i, s_i) \leftarrow (\ell, s)$ (store the current quantum numbers), and increment i.

7: **end while**

Note that although the underlying Hilbert space is complex, all steps involve real-valued matrix representations of the operators $L_z, S_z, L_\pm, S_\pm$ only. Thus, the whole algorithm can be implemented on the real numbers.

The L_z-S_z quantum numbers (including multiplicities) are sufficient to calculate the (ℓ_i, s_i) quantum numbers in Eq. (1.6), see Algorithm 1. Since each irreducible LS space contains exactly one vector in the "central" simultaneous L_z-S_z eigenspace with eigenvalues $(0,0)$ (n even) or $(0, \frac{1}{2})$ (n odd) and multiplicity $d_{u,n}$, there are exactly $d_{u,n}$ irreducible LS spaces.

Algorithm 2 actually performs the simultaneous diagonalization. It requires the (ℓ_i, s_i) tuples computed by Algorithm 1.

Algorithm 2 Simultaneous diagonalization of the operators (1.1) on $\wedge^n V_u$, yielding the decomposition (1.5)

Require: Irreducible representation space quantum numbers (ℓ_i, s_i) as computed by Algorithm 1.

1: Partition the canonical Slater determinant basis of $\wedge^n V_u$ into simultaneous L_z-S_z eigenspaces denoted W_{m_ℓ, m_s}. That is, W_{m_ℓ, m_s} is the eigenspace corresponding to eigenvalues m_ℓ and m_s, respectively.

2: **for** $i = 1, 2, \cdots$ **do**

3:    Select a (normalized) $\psi_i \in W_{\ell_i, s_i}$ and span the corresponding irreducible representation space $V_{u,n,i}$ in (1.5) by repeatedly applying the lowering operators L_- and S_-. That is,

$$V_{u,n,i} := \mathrm{span}\left\{\psi_i^{m_\ell, m_s}\right\}_{m_\ell = \ell_i, \cdots, -\ell_i, m_s = s_i, \cdots, -s_i} \quad \text{with}$$

$$\psi_i^{\ell_i, s_i} := \psi_i \quad \text{and}$$

$$\psi_i^{m_\ell - 1, m_s} := c_{\ell_i, m_\ell} L_- \psi_i^{m_\ell, m_s},$$

$$\psi_i^{m_\ell, m_s - 1} := c_{s_i, m_s} S_- \psi_i^{m_\ell, m_s}$$

and the normalization factors $c_{\ell, m} := (\ell(\ell+1) - m(m-1))^{-1/2}$.

4:    Remove the vectors spanning $V_{u,n,i}$ from any corresponding L_z-S_z eigenspace W_{ℓ_j, s_j} with $\ell_j \leq \ell_i$ and $s_j \leq s_i$. More precisely, update W_{ℓ_j, s_j} such that it contains the orthogonal complement of $\psi_i^{\ell_j, s_j}$ in W_{ℓ_j, s_j}.

5: **end for**

The basis vectors spanning the orthogonal complement in W_{ℓ_j, s_j} (line 4) are not unique. This poses a practical problem for symbolic computer algebra implementations. Namely, orthonormalizing these basis vectors can lead to a blow-up of nested squares, which is particularly unfavorable since subsequently the lowering operators (line 3) are applied to these vectors. To circumvent this difficulty, one can instead work with the unique projection matrix P_j acting on the basis vectors initially in W_{ℓ_j, s_j}. Then, in line 4, P_j is updated such that it spans precisely the orthogonal complement:

$$P_j \leftarrow P_j - \left|\psi_i^{\ell_j, s_j}\right\rangle \left\langle\psi_i^{\ell_j, s_j}\right|. \tag{2.2}$$

At the beginning, each P_j starts as identity matrix (on W_{ℓ_j, s_j}), and ends as zero matrix.

3   Example decompositions

Explicit decompositions of $\wedge^n V_f$ for $n=1,2,3$ are shown in Table 1. We have omitted $\wedge^n V_u$, $u=$s,p,d since these are already published in [7]. The complete tables are available online, including a Mathematica implementation of the algorithm [8] which makes use of the FermiFab toolbox [9,10]. For conciseness, only states with maximal L_z and S_z quantum

Table 1: Irreducible LS eigenspace decompositions of $\wedge^n V_f$ for $n=1,2,3$, see Eq. (1.5). For conciseness, the table shows states with maximal L_z and S_z quantum numbers only.

config	sym	L_z	S_z	Ψ
$\wedge^1 V_f$	$^2F^o$	3	$\frac{1}{2}$	$\lvert f_3 \rangle$
$\wedge^2 V_f$	^1I	6	0	$\lvert f_3\overline{f_3} \rangle$
	^3H	5	1	$\lvert f_3 f_2 \rangle$
	^1G	4	0	$\frac{1}{\sqrt{11}}\left(-\sqrt{3}\cdot\lvert f_3\overline{f_1}\rangle + \sqrt{3}\cdot\lvert \overline{f_3}f_1\rangle + \sqrt{5}\cdot\lvert f_2\overline{f_2}\rangle\right)$
	^3F	3	1	$\frac{1}{\sqrt{3}}\left(-\lvert f_3 f_0\rangle + \sqrt{2}\cdot\lvert f_2 f_1\rangle\right)$
	^1D	2	0	$\frac{1}{\sqrt{42}}\left(\sqrt{5}\cdot\lvert f_3\overline{f_{-1}}\rangle - \sqrt{5}\cdot\lvert \overline{f_3}f_{-1}\rangle - \sqrt{10}\cdot\lvert f_2\overline{f_0}\rangle + \sqrt{10}\cdot\lvert \overline{f_2}f_0\rangle + 2\sqrt{3}\cdot\lvert f_1\overline{f_1}\rangle\right)$
	^3P	1	1	$\frac{1}{\sqrt{14}}\left(\sqrt{3}\cdot\lvert f_3 f_{-2}\rangle - \sqrt{5}\cdot\lvert f_2 f_{-1}\rangle + \sqrt{6}\cdot\lvert f_1 f_0\rangle\right)$
	^1S	0	0	$\frac{1}{\sqrt{7}}\left(-\lvert f_3\overline{f_{-3}}\rangle + \lvert \overline{f_3}f_{-3}\rangle + \lvert f_2\overline{f_{-2}}\rangle - \lvert \overline{f_2}f_{-2}\rangle - \lvert f_1\overline{f_{-1}}\rangle + \lvert \overline{f_1}f_{-1}\rangle + \lvert f_0\overline{f_0}\rangle\right)$
$\wedge^3 V_f$	$^2K^o$	8	$\frac{1}{2}$	$\lvert f_3\overline{f_3}f_2\rangle$
	$^2J^o$	7	$\frac{1}{2}$	$\frac{1}{2\sqrt{2}}\left(\sqrt{3}\cdot\lvert f_3\overline{f_3}f_1\rangle + \sqrt{5}\cdot\lvert f_3 f_2\overline{f_2}\rangle\right)$
	$^4I^o$	6	$\frac{3}{2}$	$\lvert f_3 f_2 f_1\rangle$
	$^2I^o$	6	$\frac{1}{2}$	$\frac{1}{\sqrt{21}}\left(3\cdot\lvert f_3\overline{f_3}f_0\rangle - \sqrt{2}\cdot\lvert f_3 f_2\overline{f_1}\rangle - \sqrt{2}\cdot\lvert f_3\overline{f_2}f_1\rangle + 2\sqrt{2}\cdot\lvert \overline{f_3}f_2 f_1\rangle\right)$
	$^2H^o$	5	$\frac{1}{2}$	$\frac{1}{\sqrt{6}}\left(\sqrt{2}\cdot\lvert f_3\overline{f_3}f_{-1}\rangle - \lvert f_3\overline{f_2}f_0\rangle + \lvert \overline{f_3}f_2 f_0\rangle + \sqrt{2}\cdot\lvert f_2\overline{f_2}f_1\rangle\right)$
	$^2H^o$	5	$\frac{1}{2}$	$\frac{1}{\sqrt{273}}\left(-\sqrt{5}\cdot\lvert f_3\overline{f_3}f_{-1}\rangle - 3\sqrt{10}\cdot\lvert f_3 f_2\overline{f_0}\rangle + 2\sqrt{10}\cdot\lvert f_3\overline{f_2}f_0\rangle + 6\sqrt{3}\cdot\lvert f_3 f_1\overline{f_1}\rangle + \sqrt{10}\cdot\lvert \overline{f_3}f_2 f_0\rangle + 2\sqrt{5}\cdot\lvert f_2\overline{f_2}f_1\rangle\right)$
	$^4G^o$	4	$\frac{3}{2}$	$\frac{1}{\sqrt{11}}\left(-\sqrt{5}\cdot\lvert f_3 f_2 f_{-1}\rangle + \sqrt{6}\cdot\lvert f_3 f_1 f_0\rangle\right)$
	$^2G^o$	4	$\frac{1}{2}$	$\frac{1}{7\sqrt{5}}\left(5\sqrt{3}\cdot\lvert f_3\overline{f_3}f_{-2}\rangle + \sqrt{5}\cdot\lvert f_3 f_2\overline{f_{-1}}\rangle - 3\sqrt{5}\cdot\lvert f_3\overline{f_2}f_{-1}\rangle - \sqrt{6}\cdot\lvert f_3 f_1\overline{f_0}\rangle + \sqrt{6}\cdot\lvert f_3\overline{f_1}f_0\rangle + 2\sqrt{5}\cdot\lvert \overline{f_3}f_2 f_{-1}\rangle + 2\sqrt{10}\cdot\lvert f_2\overline{f_2}f_0\rangle + 4\sqrt{3}\cdot\lvert f_2 f_1\overline{f_1}\rangle\right)$

Table 1: (cont'd) Irreducible LS eigenspace decompositions of $\wedge^n V_f$ for $n=1,2,3$, see Eq. (1.5). For conciseness, the table shows states with maximal L_z and S_z quantum numbers only.

config	sym	L_z	S_z	Ψ
$\wedge^3 V_f$	$^2G^o$	4	$\frac{1}{2}$	$\frac{1}{7\sqrt{429}}\left(-18\sqrt{6}\cdot\left\vert f_3\overline{f_3}f_{-2}\right\rangle+16\sqrt{10}\cdot\left\vert f_3f_2\overline{f_{-1}}\right\rangle+\sqrt{10}\cdot\left\vert f_3\overline{f_2}f_{-1}\right\rangle-32\sqrt{3}\cdot\left\vert f_3f_1\overline{f_0}\right\rangle\right.$ $-17\sqrt{3}\cdot\left\vert f_3\overline{f_1}f_0\right\rangle-17\sqrt{10}\cdot\left\vert \overline{f_3}f_2f_{-1}\right\rangle+49\sqrt{3}\cdot\left\vert \overline{f_3}f_1f_0\right\rangle+15\sqrt{5}\cdot\left\vert f_2\overline{f_2}f_0\right\rangle$ $\left.+15\sqrt{6}\cdot\left\vert f_2f_1\overline{f_1}\right\rangle\right)$
	$^4F^o$	3	$\frac{3}{2}$	$\frac{1}{2}\left(\left\vert f_3f_2f_{-2}\right\rangle-\left\vert f_3f_1f_{-1}\right\rangle+\sqrt{2}\cdot\left\vert f_2f_1f_0\right\rangle\right)$
	$^2F^o$	3	$\frac{1}{2}$	$\frac{1}{\sqrt{6}}\left(\left\vert f_3\overline{f_3}f_{-3}\right\rangle+\left\vert f_3f_2\overline{f_{-2}}\right\rangle-\left\vert f_3\overline{f_2}f_{-2}\right\rangle-\left\vert f_3f_1\overline{f_{-1}}\right\rangle\right.$ $\left.+\left\vert f_3\overline{f_1}f_{-1}\right\rangle+\left\vert f_3f_0\overline{f_0}\right\rangle\right)$
	$^2F^o$	3	$\frac{1}{2}$	$\frac{1}{2\sqrt{33}}\left(7\cdot\left\vert f_3\overline{f_3}f_{-3}\right\rangle-3\cdot\left\vert f_3f_2\overline{f_{-2}}\right\rangle-2\cdot\left\vert f_3\overline{f_2}f_{-2}\right\rangle+3\cdot\left\vert f_3f_1\overline{f_{-1}}\right\rangle\right.$ $-\left\vert f_3\overline{f_1}f_{-1}\right\rangle-2\cdot\left\vert f_3f_0\overline{f_0}\right\rangle+5\cdot\left\vert \overline{f_3}f_2f_{-2}\right\rangle-2\cdot\left\vert \overline{f_3}f_1f_{-1}\right\rangle$ $\left.+\sqrt{15}\cdot\left\vert f_2\overline{f_2}f_{-1}\right\rangle-\sqrt{2}\cdot\left\vert f_2f_1\overline{f_0}\right\rangle-\sqrt{2}\cdot\left\vert f_2\overline{f_1}f_0\right\rangle+2\sqrt{2}\cdot\left\vert \overline{f_2}f_1f_0\right\rangle\right)$
	$^4D^o$	2	$\frac{3}{2}$	$\frac{1}{\sqrt{21}}\left(\sqrt{10}\cdot\left\vert f_3f_2f_{-3}\right\rangle-\sqrt{6}\cdot\left\vert f_3f_1f_{-2}\right\rangle+\sqrt{5}\cdot\left\vert f_3f_0f_{-1}\right\rangle\right)$
	$^2D^o$	2	$\frac{1}{2}$	$\frac{1}{2\sqrt{42}}\left(2\sqrt{5}\cdot\left\vert f_3f_2\overline{f_{-3}}\right\rangle-\sqrt{5}\cdot\left\vert f_3\overline{f_2}f_{-3}\right\rangle-2\sqrt{3}\cdot\left\vert f_3f_1\overline{f_{-2}}\right\rangle-\sqrt{3}\cdot\left\vert f_3\overline{f_1}f_{-2}\right\rangle\right.$ $+\sqrt{10}\cdot\left\vert f_3f_0\overline{f_{-1}}\right\rangle+\sqrt{10}\cdot\left\vert f_3\overline{f_0}f_{-1}\right\rangle-\sqrt{5}\cdot\left\vert \overline{f_3}f_2f_{-3}\right\rangle+3\sqrt{3}\cdot\left\vert \overline{f_3}f_1f_{-2}\right\rangle$ $-2\sqrt{10}\cdot\left\vert \overline{f_3}f_0f_{-1}\right\rangle+2\sqrt{5}\cdot\left\vert f_2\overline{f_2}f_{-2}\right\rangle-\sqrt{5}\cdot\left\vert f_2\overline{f_1}f_{-1}\right\rangle+\sqrt{5}\cdot\left\vert \overline{f_2}f_1f_{-1}\right\rangle$ $\left.+\sqrt{6}\cdot\left\vert f_1\overline{f_1}f_0\right\rangle\right)$
	$^2D^o$	2	$\frac{1}{2}$	$\frac{1}{6\sqrt{154}}\left(-14\sqrt{5}\cdot\left\vert f_3f_2\overline{f_{-3}}\right\rangle+7\sqrt{5}\cdot\left\vert f_3\overline{f_2}f_{-3}\right\rangle+14\sqrt{3}\cdot\left\vert f_3f_1\overline{f_{-2}}\right\rangle-13\sqrt{3}\cdot\left\vert f_3\overline{f_1}f_{-2}\right\rangle\right.$ $-\sqrt{10}\cdot\left\vert f_3f_0\overline{f_{-1}}\right\rangle+5\sqrt{10}\cdot\left\vert f_3\overline{f_0}f_{-1}\right\rangle+7\sqrt{5}\cdot\left\vert \overline{f_3}f_2f_{-3}\right\rangle-\sqrt{3}\cdot\left\vert \overline{f_3}f_1f_{-2}\right\rangle$ $-4\sqrt{10}\cdot\left\vert \overline{f_3}f_0f_{-1}\right\rangle+6\sqrt{5}\cdot\left\vert f_2\overline{f_2}f_{-2}\right\rangle-12\sqrt{5}\cdot\left\vert f_2f_1\overline{f_{-1}}\right\rangle+3\sqrt{5}\cdot\left\vert f_2\overline{f_1}f_{-1}\right\rangle$ $\left.+12\sqrt{5}\cdot\left\vert f_2f_0\overline{f_0}\right\rangle+9\sqrt{5}\cdot\left\vert \overline{f_2}f_1f_{-1}\right\rangle+9\sqrt{6}\cdot\left\vert f_1\overline{f_1}f_0\right\rangle\right)$
	$^2P^o$	1	$\frac{1}{2}$	$\frac{1}{2\sqrt{21}}\left(\sqrt{6}\cdot\left\vert f_3\overline{f_1}f_{-3}\right\rangle+\sqrt{3}\cdot\left\vert f_3f_0\overline{f_{-2}}\right\rangle-2\sqrt{3}\cdot\left\vert f_3\overline{f_0}f_{-2}\right\rangle-\sqrt{10}\cdot\left\vert f_3f_{-1}\overline{f_{-1}}\right\rangle\right.$ $-\sqrt{6}\cdot\left\vert \overline{f_3}f_1f_{-3}\right\rangle+\sqrt{3}\cdot\left\vert \overline{f_3}f_0f_{-2}\right\rangle-\sqrt{10}\cdot\left\vert f_2\overline{f_2}f_{-3}\right\rangle-\sqrt{6}\cdot\left\vert f_2f_1\overline{f_{-2}}\right\rangle$ $+\sqrt{6}\cdot\left\vert f_2\overline{f_1}f_{-2}\right\rangle+\sqrt{5}\cdot\left\vert f_2f_0\overline{f_{-1}}\right\rangle-\sqrt{5}\cdot\left\vert \overline{f_2}f_0f_{-1}\right\rangle-\sqrt{6}\cdot\left\vert f_1\overline{f_1}f_{-1}\right\rangle$ $\left.-\sqrt{6}\cdot\left\vert f_1f_0\overline{f_0}\right\rangle\right)$
	$^4S^o$	0	$\frac{3}{2}$	$\frac{1}{\sqrt{7}}\left(-\left\vert f_3f_0f_{-3}\right\rangle+\sqrt{2}\cdot\left\vert f_3f_{-1}f_{-2}\right\rangle+\sqrt{2}\cdot\left\vert f_2f_1f_{-3}\right\rangle-\left\vert f_2f_0f_{-2}\right\rangle+\left\vert f_1f_0f_{-1}\right\rangle\right)$

numbers are displayed; applying the lowering operators L_- and S_- yields the remaining wavefunctions. Note that in general, symmetry levels can appear more than once within a many-particle subshell, e.g., $^2G^o$ in $\wedge^3 V_f$. Thus, the tables are only unique up to (orthogonal) base changes of the states within the same symmetry level. The run time on a commodity laptop computer to calculate the symbolic eigenspaces is approximately 16 seconds for $u = f$ and $n = 3$, and 550 seconds for $u = f$ and $n = 4$.

4   Complexity analysis

This section contains a derivation of Eqs. (1.7) and (1.8) in the limit of fixed electron number n and $u \to \infty$.

We first investigate the multiplicity distribution of the simultaneous L_z-S_z eigenvalues, as illustrated in Fig. 2. In the following, $T(m_\ell, m_s)$ denotes the multiplicity of the simultaneous L_z-S_z eigenspace with eigenvalues (m_ℓ, m_s) on $\wedge^n V_u$. We write $[\cdot]$ for the nearest integer function. Furthermore, $f_{\text{IH},n}$ and $f_{\text{bin},n,p}$ denote the probability density functions of the standard Irwin-Hall distribution [11, 12] (sum of n i.i.d. $U(0,1)$ random variables) and the binomial distribution with parameters (n,p), respectively.
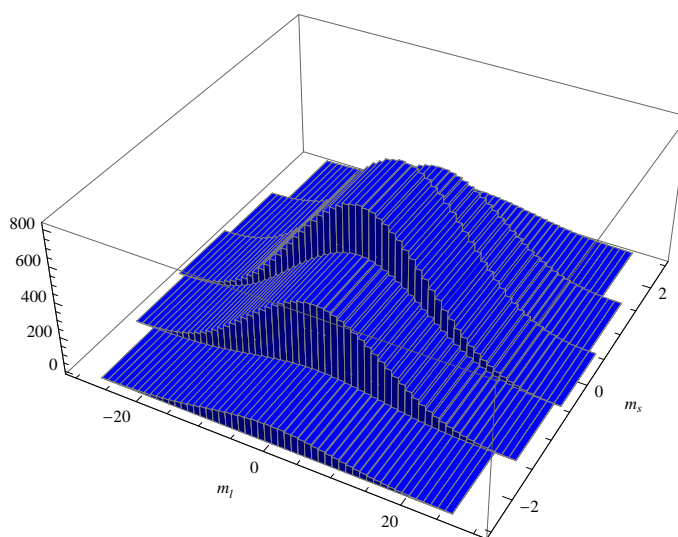

Figure 2: Histogram plot of the L_z-S_z eigenvalue multiplicities of $\wedge^4 V_8$. This is equivalent to the table in Fig. 1 but for $u = 8$ and $n = 4$. The probability density function approaches a normal distribution as a result of the central limit theorem for large n; compare with Proposition 4.1.

Proposition 4.1. Given a fixed integer $n \geq 1$, define

$$t_{u,n}(x_\ell, m_s) := \frac{u\, T([u\, x_\ell], m_s)}{\dim(\wedge^n V_u)}, \quad x_\ell \in [-n, n], \quad m_s \in \{n/2, \cdots, -n/2\}. \tag{4.1}$$

Then for each m_s,

$$\lim_{u\to\infty} t_{u,n}(x_\ell, m_s) = f_{L_z}(x_\ell) f_{S_z}(m_s) \tag{4.2}$$

uniformly in x_ℓ with

$$f_{L_z}(x_\ell) := \frac{1}{2} f_{\text{IH},n}\left(\frac{x_\ell}{2} + \frac{n}{2}\right), \quad f_{S_z}(m_s) := f_{\text{bin},n,\frac{1}{2}}\left(m_s + \frac{n}{2}\right). \tag{4.3}$$

In particular, f_{L_z} and f_{S_z} have zero mean and variances $\sigma_\ell^2 = n/3$ and $\sigma_s^2 = n/4$, respectively.

The factor u in the definition of $t_{u,n}$ ensures normalization in the sense that

$$\sum_{m_s} \int_{[-n,n]} t_{u,n}(x_\ell, m_s) \, dx_\ell = \dim(\wedge^n V_u)^{-1} \sum_{m_s} \int_{[-nu,nu]} T([m_\ell], m_s) \, dm_\ell$$

$$\cong \dim(\wedge^n V_u)^{-1} \sum_{m_\ell, m_s} T(m_\ell, m_s) = 1. \tag{4.4}$$

Proof. First label the basis vectors ("spherical harmonics") spanning V_u abstractly as

$$Y_u := \{u\uparrow, u\downarrow, \cdots, (-u)\uparrow, (-u)\downarrow\}. \tag{4.5}$$

Now let $\psi = |\varphi_1, \cdots, \varphi_n\rangle \in \wedge^n V_u$ be a uniformly random Slater determinant, with $\varphi_i \in Y_u$ pairwise different. In other words, ψ randomly selects n distinct elements from Y_u. As already shown in the beginning of Section 2, ψ is a simultaneous L_z-S_z eigenvector. To estimate the distribution $(\text{eig}_{L_z}(\psi), \text{eig}_{S_z}(\psi))$, note that L_z and S_z just sum up the corresponding terms in ψ. Thus, for example,

$$\text{eig}_{L_z}(|2\uparrow, 1\downarrow, -1\uparrow\rangle) = 2 + 1 - 1 = 2, \tag{4.6}$$

$$\text{eig}_{S_z}(|2\uparrow, 1\downarrow, -1\uparrow\rangle) = \tfrac{1}{2} - \tfrac{1}{2} + \tfrac{1}{2} = \tfrac{1}{2}. \tag{4.7}$$

Observe that the error incurred by ignoring the exclusion principle goes to zero as $u \to \infty$ due to $n \ll u$. That is, we may replace ψ by $\tilde{\psi} := \tilde{\varphi}_1 \otimes \cdots \otimes \tilde{\varphi}_n \in \bigotimes^n V_u$ with $\tilde{\varphi}_i \in Y_u$ i.i.d. (independent and identically distributed). Then $\text{eig}_{L_z}(\tilde{\psi})$ and $\text{eig}_{S_z}(\tilde{\psi})$ are independent as well and can be handled separately. The distribution f_{S_z} stems directly from $\text{eig}_{S_z}(\tilde{\psi}) = \sum_i \text{eig}_{S_z}(\tilde{\varphi}_i)$. Considering $\text{eig}_{L_z}(\tilde{\psi})$, first note that the discretization error

$$\left| f_{L_z}(x_\ell) - f_{L_z}\left(\frac{[u x_\ell]}{u}\right) \right| \to 0 \tag{4.8}$$

as $u \to \infty$ since f_{L_z} is uniformly continuous. Thus, the distribution of $\frac{1}{u} \text{eig}_{L_z}(\tilde{\varphi}_i)$ approaches $U(-1,1)$, and consequently, $\frac{1}{u} \text{eig}_{L_z}(\tilde{\psi}) = \sum_i \frac{1}{u} \text{eig}_{L_z}(\tilde{\varphi}_i) \sim f_{L_z}$. $\square$

4.1 Run time

This subsection is concerned with the asymptotic run time of the main algorithm, as already stated in the introduction.

Proposition 4.2. For any fixed integer $n \geq 1$, the run time $R_n(u)$ of Algorithm 2 obeys

$$R_n(u) = \mathcal{O}(u^{3n-2}) \tag{4.9}$$

as $u \to \infty$.

Proof. Due to the sparse matrix structure of the lowering operators L_- and S_-, each matrix multiplication in line 3 of the algorithm has linear (instead of quadratic) cost. Thus, the main computational cost stems from line 4. Denote the tuples (ℓ_i, s_i) after deleting duplicates by (ℓ'_k, s'_k). For each simultaneous L_z-S_z eigenspace $W_{\ell'_k, s'_k}$ with dimension $d_k := \dim(W_{\ell'_k, s'_k})$, the algorithm calculates d_k orthogonal complements within $W_{\ell'_k, s'_k}$, each of which takes $\mathcal{O}(d_k^2)$ operations. So in total, $R_n(u) = \mathcal{O}(\sum_k d_k^3)$. Combining this result with (4.2) yields the following upper bound,

$$
\begin{aligned}
R_n(u) &\lesssim \frac{1}{4} \dim(\wedge^n V_u)^3 \int_{[-nu,nu]} u^{-3} f_{L_z}(m_\ell/u)^3 \mathrm{d}m_\ell \sum_{m_s} f_{S_z}(m_s)^3 \\
&= \frac{1}{4} \dim(\wedge^n V_u)^3 u^{-2} \int_{\mathbb{R}} f_{\mathrm{IH},n}(x_\ell)^3 \mathrm{d}x_\ell \sum_{x_s=0}^{n} f_{\mathrm{bin},n,\frac{1}{2}}(x_s)^3 \\
&= \mathcal{O}(u^{3n-2}).
\end{aligned} \tag{4.10}
$$

The factor $\frac{1}{4}$ stems from the observation that for each k, neither $W_{\ell'_k, -s'_k}$, $W_{-\ell'_k, s'_k}$ nor $W_{-\ell'_k, -s'_k}$ contribute to the cost. The second line follows from a change of variables, and the third from noting that the integral and sum in the second line do not depend on u. $\square$

Taking one step further, we can now investigate the dependency of $R_n(u)$ on n in more detail and evaluate the terms in the second line of (4.10). We obtain the following:

Lemma 4.1. *Assume that n is large enough such that f_{L_z} and f_{S_z} can be well approximated by Gaussian normal distributions with mean 0 and variances σ_ℓ and σ_s from Proposition* 4.1. *Then*

$$R_n(u) \lesssim \frac{\dim(\wedge^n V_u)^3}{48\pi^2 u^2 \sigma_\ell^2 \sigma_s^2} = \frac{\dim(\wedge^n V_u)^3}{(2\pi nu)^2}. \tag{4.11}$$

4.2 Dimension of the central L_z-S_z eigenspace

Let $d_{u,n}$ label the maximum dimension of any simultaneous L_z-S_z eigenspace on $\wedge^n V_u$, which is attained by the "central" eigenspace with eigenvalues $(m_\ell, m_s) = (0,0)$ for n even and $(0,\frac{1}{2})$ for n odd, respectively. Thus, $d_{u,n}$ can be approximated by evaluating the right side of Eq. (4.2) at these eigenvalues. A comparison with the exact $d_{u,n}$
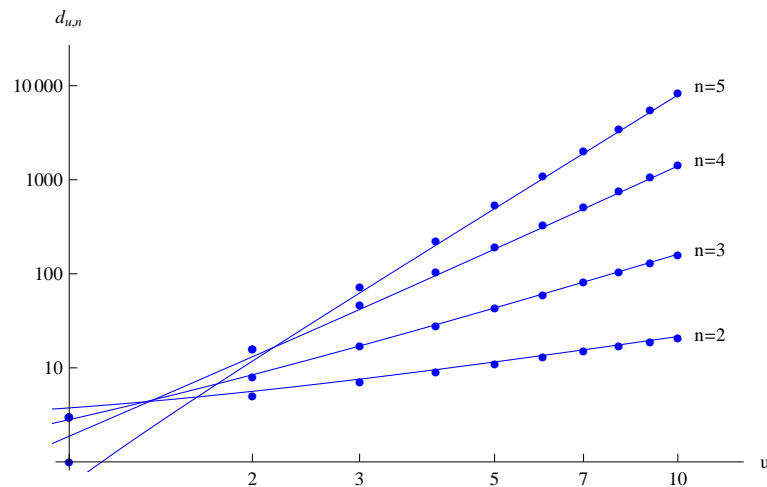
Figure 3: Log-log plot of $d_{u,n}$ versus u for various n. Dots are exact values, and lines show the right side of Eq. (4.2) evaluated at $(m_\ell, m_s) = (0,0)$ for n even and $(0, \frac{1}{2})$ for n odd, respectively.

is shown in Fig. 3, which nicely illustrates the polynomial scaling in u. As a remark, $f_{\text{IH},n}(\frac{n}{2}) = \frac{2}{\pi} \int_0^\infty \text{sinc}(x)^n \, dx$ due to the convolution theorem applied to the uniform probability density function on the interval $[-1/2, 1/2]$.

To derive Eq. (1.8), we follow the same procedure as above and replace f_{L_z} and f_{S_z} by Gaussian normal distributions. We then set $m_s = 0$ both for n even and n odd since $\frac{1}{2}$ is small compared to n. Plugging in $(m_\ell, m_s) = (0,0)$ yields

Lemma 4.2. *Assume that n is large enough such that f_{L_z} and f_{S_z} can well be approximated by Gaussian normal distributions. Then*

$$d_{u,n} \cong \frac{\dim(\wedge^n V_u)}{2\pi u \sigma_\ell \sigma_s} = \sqrt{3} \, \frac{\dim(\wedge^n V_u)}{\pi n u}. \tag{4.12}$$

5 Conclusions

The main principle of the algorithm is the *implicit* simultaneous diagonalization of the many-particle angular momentum, spin and parity operators by algebraic traversal of the L_z-S_z eigenstates in the correct order. This involves $\mathcal{O}(u^{3n-2})$ operations for angular subshell u filled with n electrons. When taking any admissible n into account, subshells up to $u = d$ are feasible at present, and $u = f$ for all $n = 1, \cdots, 14$ might still be attainable. Notably, the electronic ground state configurations found in the periodic table are precisely constructed from the atomic s, p, d, f subshells.

Acknowledgments

References

[1] C. Froese Fischer, T. Brage, and P. Johnsson. *Computational atomic structure: An MCHF approach*. CRC Press, 1997.

[2] S. Fraga, J. Karwowski, and K. M. S. Saxena. *Handbook of atomic data*. Elsevier, 1976.

[3] C. W. Bauschlicher and P. R. Taylor. Benchmark full configuration-interaction calculations on H_2O, F, and F^-. *J. Chem. Phys.*, 85(5):2779–2783, 1986.

[4] M. Chaichian and R. Hagedorn. *Symmetries in quantum mechanics: from angular momentum to supersymmetry*. CRC Press, 1997.

[5] G. Friesecke and B. D. Goddard. Explicit large nuclear charge limit of electronic ground states for Li, Be, B, C, N, O, F, Ne and basic aspects of the periodic table. *SIAM J. Math. Anal.*, 41(2):631–664, 2009.

[6] G. Friesecke and B. D. Goddard. Asymptotics-based CI models for atoms: properties, exact solution of a minimal model for Li to Ne, and application to atomic spectra. *Multiscale Model. Simul.*, 7(4):1876–1897, 2009.

[7] C. B. Mendl and G. Friesecke. Efficient algorithm for asymptotics-based configuration-interaction methods and electronic structure of transition metal atoms. *J. Chem. Phys.*, 133:184101, 2010.

[8] C. B. Mendl. `https://github.com/cmendl/irredLS`, 2009–2014.

[9] C. B. Mendl. The FermiFab toolbox for fermionic many-particle quantum systems. *Comput. Phys. Commun.*, 182:1327–1337, 2011.

[10] C. B. Mendl. FermiFab Matlab/Mathematica toolbox software, online at `http://sourceforge.net/projects/fermifab`, 2008–2014.

[11] J. O. Irwin. On the frequency distribution of the means of samples from a population having any law of frequency with finite moments, with special reference to Pearson's type II. *Biometrika*, 19:225–239, 1927.

[12] P. Hall. The distribution of means for samples of size N drawn from a population in which the variate takes values between 0 and 1, all such values being equally probable. *Biometrika*, 19:240–245, 1927.